

Supplementary material to:

Optical and biogeochemical properties of Belgian inland and coastal waters

Alexandre Castagna, Luz Amadei Martínez, Margarita Bogorad, Ilse Daveloose,
Renaat Dassevile, Heidi Dierssen, Matthew Beck, Jonas Mortelmans, Héloïse
Lavigne, Ana Dogliotti, David Doxaran, Kevin Ruddick, Wim Vyverman, and
Koen Sabbe

Earth System Science Data, *x*, *x–x*, 2022

doi: *x*

Figure S1

Evaluation of the salinity effect on the determination of a_g from contrasting limits (salinity of 0 and 35). Absolute values are expressed in terms of attenuation coefficient, c , as they include the optical effects of the quartz cuvette (baseline in air). The difference of the attenuation from artificial seawater to pure water was subtracted from a_g of marine and brackish samples for an approximate correction.

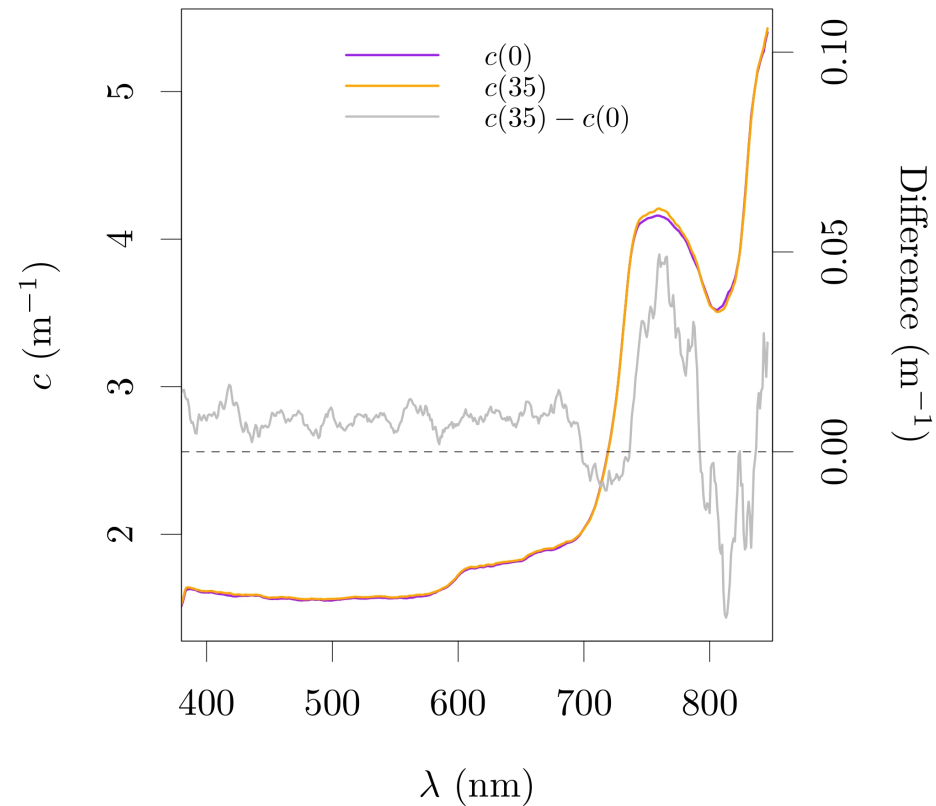


Figure S2

Example of samples for determination of particle absorption coefficient. Sample of station ZL_03 shows cyanobacterial filamentous colonies forming non-homogeneous deposition on the filter surface. The filter is shown before and after the pigment chemical oxidation with sodium hypochlorite.

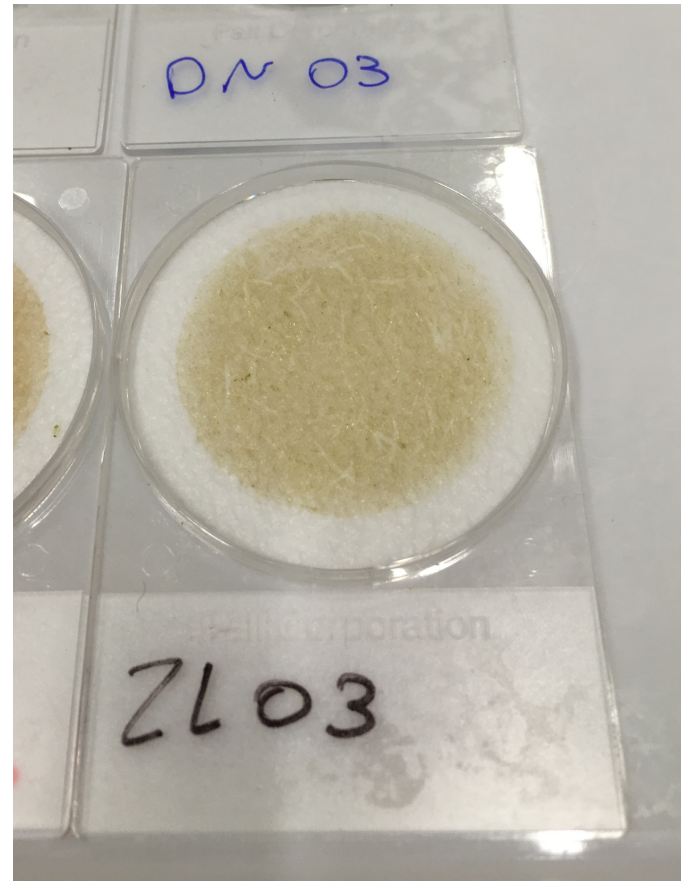


Figure S3

Evaluation of the salinity effect on the determination of c_{nw} from contrasting limits (salinity of 0 and 35). Absolute values are expressed in terms of attenuation coefficient, c , as they include the optical effects of the quartz cuvette (baseline in air). The difference of the attenuation from artificial seawater to pure water was subtracted from c_{nw} of marine and brackish samples for an approximate correction.

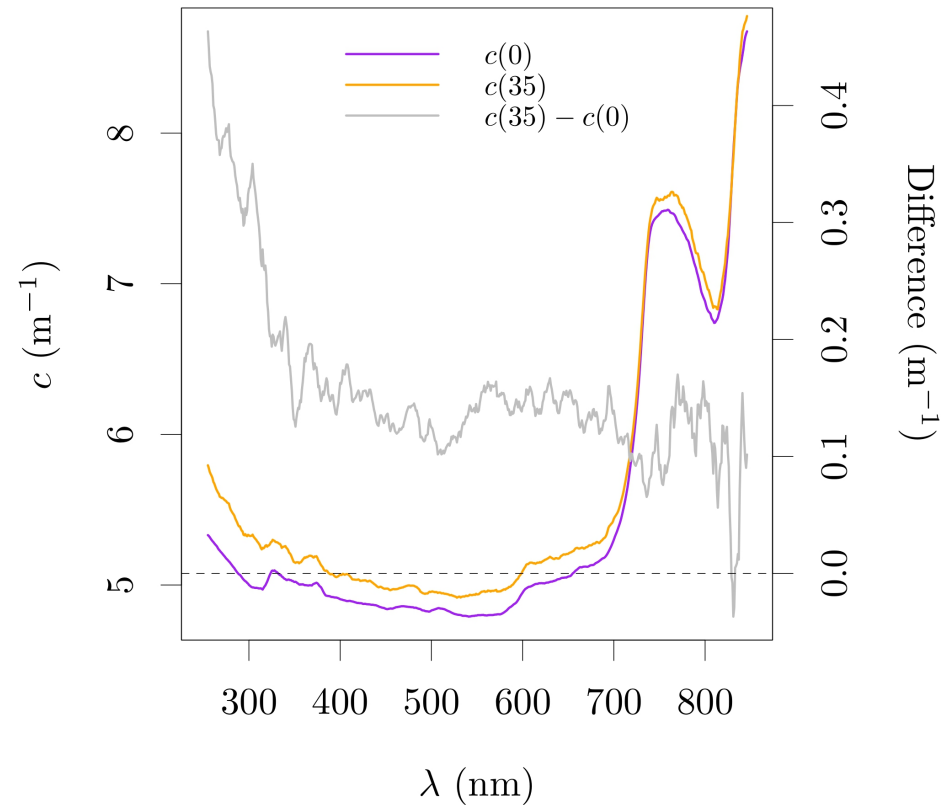


Figure S4

Detailed example of the validation of the particle beam attenuation coefficient, c_p , measured with the spectrophotometer at an acceptance angle of 0.074° against the values measured by the LISST instruments at an acceptance angle of 0.018° . The difference between c_p measured by the different instruments (A) is accounted by the scattering within the difference of acceptance angle of the instruments, as estimated from the particle volume scattering function, β_p (B).

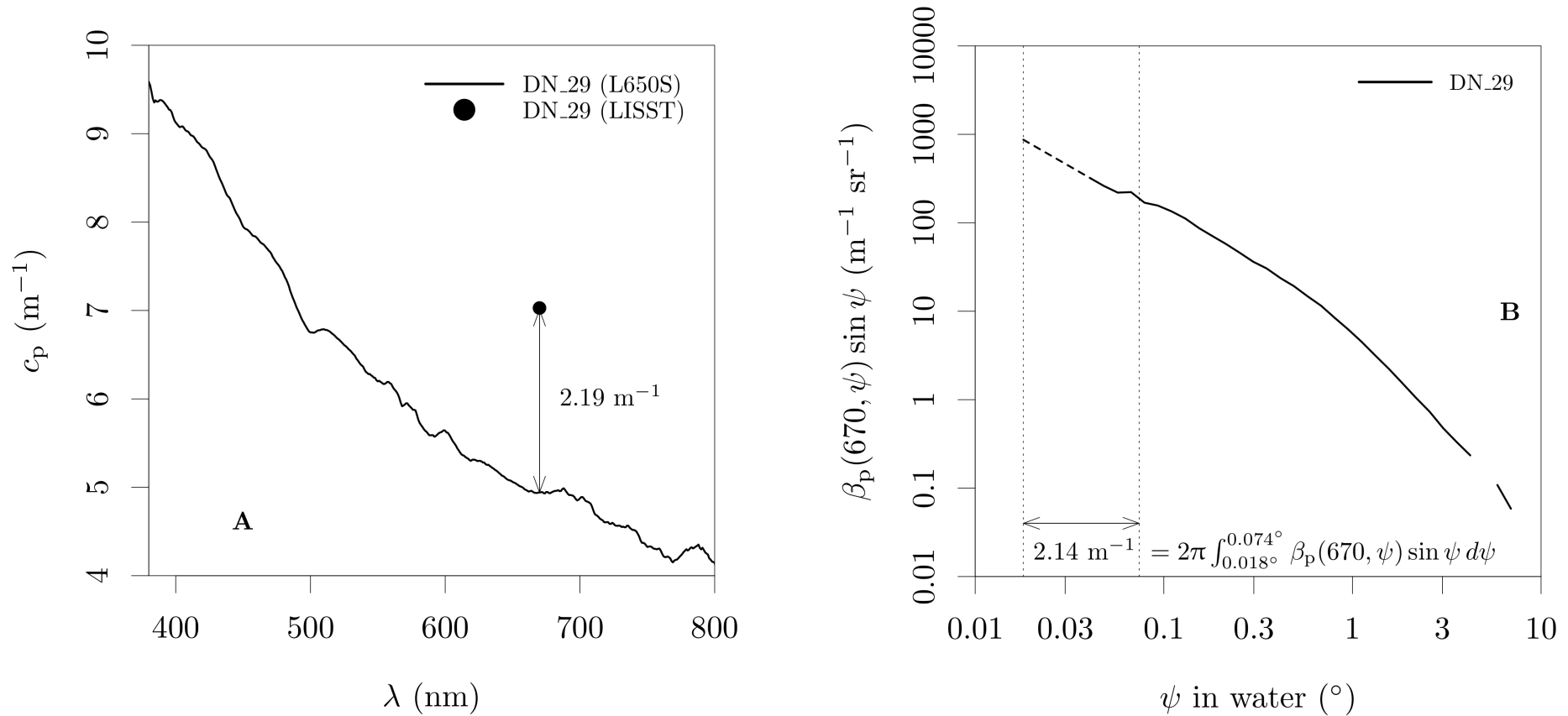


Figure S5

Example of the measurement setup for on water radiometry from small platforms using a single spectrometer. The global (direct + diffuse) downwelling plane irradiance was estimated from the exitant radiance from a reference sintered PTFE plaque, while the water leaving radiance was estimated at 0.5 m from the platform, aligned to the Sun azimuth, by placing the opening of the lens' shield at 2.5 cm below the water surface.



Figure S6

Example of the shadowing simulations calculated for the setup of the measurements of reflectance spectroscopy using the on water method. The example here shows the shadowing for the diffuse fraction with the Sun at 30° zenith angle (clear skies; Castagna et al., 2019) and optically deep waters. (A) Total shadowing error as a function of the total absorption coefficient, a_t , and the total beam attenuation, c_t ; (B) The difference between the total shadowing with the shadowing caused by the tip of the lens' shield (skylight-blocking apparatus), showing that the platform shadowing (boat) is small and only relevant at low a_t values.

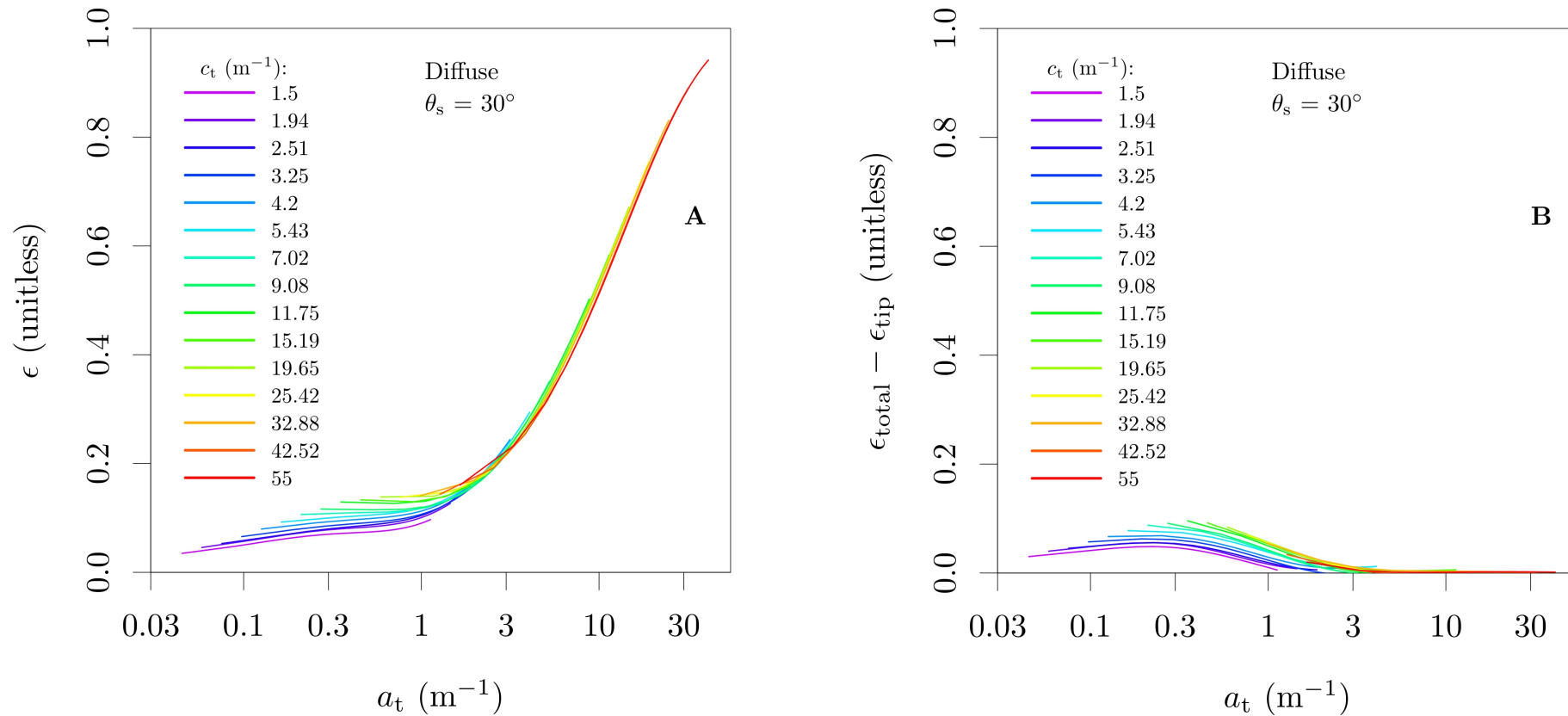


Figure S7

Example of the setup for measurement of reflectance spectroscopy of the sediment surface, sampled with cores taken from the Spuikom. Measurements were performed under a water layer of 5 cm. Note that the images show different cores.



Figure S8

Example of the floating biofilm patches observed in the Spuikom in July, 2018. Reflectance spectroscopy were performed *in situ* without disturbing the floating mats. Microscopy observations revealed an assemblage of benthic diatoms including species of the genera *Pleurosigma*, *Gyrosigma* and *Navicula*.

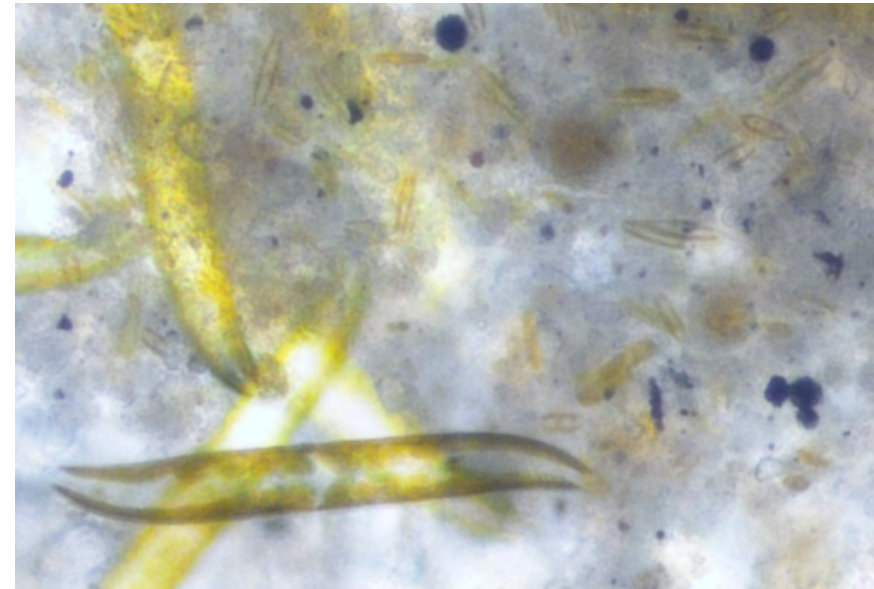


Figure S9

Example of the setup for measurements of reflectance spectroscopy of macroalgae. Description of the measurement, instruments and auxiliary materials are provided in the main text.

